Electrochimica Acta 60 (2012) 154–162

Contents lists available at SciVerse ScienceDirect

Electrochimica Acta

journal homepage: www.elsevier.com/locate/electacta

Thermodynamic properties of calcium–bismuth alloys determined by emf measurements

Hojong Kim, Dane A. Boysen, David J. Bradwell, Brice Chung, Kai Jiang, Alina A. Tomaszowska, Kangli Wang, Weifeng Wei, Donald R. Sadoway*

Department of Materials Science and Engineering, Massachusetts Institute of Technology, 77 Massachusetts Avenue, Cambridge, MA 02139-4307, USA

ARTICLE INFO

Article history:
Received 28 August 2011
Received in revised form 6 November 2011
Accepted 6 November 2011
Available online 15 November 2011

Keywords:
Calcium–bismuth alloys
Emf method
Ca–Bi binary phase diagram
Thermodynamic properties

ABSTRACT

The thermodynamic properties of Ca–Bi alloys were determined by electromotive force (emf) measurements to assess the suitability of Ca–Bi electrodes for electrochemical energy storage applications. Emf was measured at ambient pressure as a function of temperature between 723 K and 1173 K using a Ca(s)|CaF_2(s)|Ca(in Bi) cell for twenty different Ca–Bi alloys spanning the entire range of composition from $x_{Ca} = 0$ to 1. Reported are the temperature-independent partial molar entropy and enthalpy of calcium for each Ca–Bi alloy. Also given are the measured activities of calcium, the excess partial molar Gibbs energy of bismuth estimated from the Gibbs–Duhem equation, and the integral change in Gibbs energy for each Ca–Bi alloy at 873 K, 973 K, and 1073 K. Calcium activities at 973 K were found to be nearly constant at a value of $a_{Ca} = 1 \times 10^{-8}$ over the composition range $x_{Ca} = 0.32$–0.56, yielding an emf of ~0.77 V. Above $x_{Ca} = 0.62$ and coincident with Ca_5Bi_3 formation, the calcium activity approached unity. The Ca–Bi system was also characterized by differential scanning calorimetry over the entire range of composition. Based upon these data along with the emf measurements, a revised Ca–Bi binary phase diagram is proposed.

1. Introduction

The thermochemical properties of Ca–Bi alloys were investigated to determine the viability of Ca–Bi electrodes for high temperature electrochemical energy storage applications. The thermodynamic characterization of calcium-based alloys is challenging due to the high reactivity of calcium metal. Coulometric titration techniques utilizing molten salt electrolytes are often performed to measure the thermodynamic properties of alloys; however, pure calcium metal is well known to have a high solubility (up to 4 mol%) in molten salt electrolytes; this endows the electrolyte with electronic conductivity and prevents compositional accounting by coulometric titration [1,2].

Suitable solid electrolytes have greatly enhanced the range of material systems for which thermochemical data can be obtained by electromotive force (emf) methods, which lend themselves to simpler, more compact cell assemblies with either solid or liquid electrodes. Pratt has published a comprehensive review [3] on the use of solid electrolytes in thermodynamic studies.

Particularly prevalent has been the use of CaF_2 as a solid electrolyte, owing to the wide-range of activities and temperatures for which it exhibits purely ionic conduction [4]. Delcet and Egan have used cells fitted with a solid CaF_2 electrolyte to measure calcium activities of many Ca-based alloys by coulometric titration, including Ag, Au, Zn, In, Tl, Sn, Pb, Sb, and Bi as the second component [5–8]. For these measurements, care was taken to use alloys with Ca activity $a_{Ca} < 10^{-3}$, above which CaF_2 was shown to have sufficient electronic conductivity as to deviate intolerably from Nernstian behavior in open circuit measurements [9].

In a departure from the previous work by Delcet et al. [5] in which the emf was measured at a single temperature as the composition was varied by coulometric titration over calcium mole fractions with low calcium activity, in the present study emf measurements were made as a function of temperature between pure Ca metal ($a_{Ca} = 1$) and a Ca–Bi alloy of fixed calcium mole fraction x_{Ca}. Eliminating the need to change composition in situ permitted the use of a thick CaF_2 electrolyte, which minimized electronic conduction due to calcium solubility over the duration of each experiment, even at high calcium activities.

The temperature-dependent thermodynamic properties of Ca–Bi alloys were investigated using the electrochemical cell

$$\text{Ca(s)}|\text{CaF}_2\text{(s)}|\text{Ca(in Bi)}, \quad (1)$$

where solid calcium served as a reference electrode (RE), solid CaF_2 as an electrolyte, and various compositions of Ca–Bi alloys as

* Corresponding author. Tel.: +1 6172533487; fax: +1 6172535418.
E-mail address: dsadoway@mit.edu (D.R. Sadoway).

0013-4686/$ – see front matter © 2011 Elsevier Ltd. All rights reserved.
doi:10.1016/j.electacta.2011.11.023

working electrodes (WEs). Since CaF_2 is a fluoride-ion conducting electrolyte [10], the half-cell reactions are

$$\begin{aligned} &\text{RE}: \ \text{Ca(s)} + 2\text{F}^- = \text{CaF}_2\text{(s)} + 2e^- \\ &\text{WE}: \ \text{CaF}_2\text{(s)} + 2e^- = \text{Ca(in Bi)} + 2\text{F}^- \end{aligned} \tag{2}$$

and the overall cell reaction

$$\text{Ca(s)} = \text{Ca(in Bi)}. \tag{3}$$

For this reaction, the change in partial molar Gibbs energy of calcium is

$$\Delta\bar{G}_{\text{Ca}} = \bar{G}_{\text{Ca(in Bi)}} - \bar{G}_{\text{Ca(s)}}, \tag{4}$$

where for each component i the partial molar Gibbs energy, $\bar{G}_i$, is given by

$$\begin{aligned} \bar{G}_{\text{Ca(in Bi)}} &= \bar{G}^{\circ}_{\text{Ca(in Bi)}} + RT\ln a_{\text{Ca(in Bi)}} \\ \bar{G}_{\text{Ca(s)}} &= \bar{G}^{\circ}_{\text{Ca(s)}} + RT\ln a_{\text{Ca(s)}} \, (a_{\text{Ca(s)}} = 1) \end{aligned}, \tag{5}$$

where a_i is the activity, $\bar{G}^{\circ}_i$ the standard partial molar Gibbs energy, R the gas constant, and T temperature. From the Nernst equation,

$$\Delta\bar{G} = -zFE_{\text{cell}} \tag{6}$$

applied to Eqs. (4) and (5), the measured cell electromotive force E_{cell} is related to the change in partial molar Gibbs free energy of calcium by

$$E_{\text{cell}} = \frac{-\Delta\bar{G}_{\text{Ca}}}{zF} = -\left(\frac{RT}{zF}\right)\ln a_{\text{Ca(in Bi)}}, \tag{7}$$

where F is the Faraday constant and $z = 2$, the number of electrons. Notation going forward will be simplified as follows: $E_{\text{cell}} \rightarrow E$ and $X_{\text{Ca(in Bi)}} \rightarrow X_{\text{Ca}}$, where X is a generic thermodynamic variable.

At elevated temperatures and ambient pressure, pure calcium undergoes two transitions:

$$\text{Ca(cr, } Fm\bar{3}m) \underset{716\text{K}}{\overset{T_{\text{trs}}}{\longleftrightarrow}} \text{Ca(cr, } Im\bar{3}m) \underset{1115\text{K}}{\overset{T_{\text{fus}}}{\longleftrightarrow}} \text{Ca(l)}. \tag{8}$$

In this work, the high-temperature structure of calcium, Ca(cr, $Im\bar{3}m$) at each measurement temperature T (716–1115 K) and ambient pressure was selected as the standard state.

2. Experimental

2.1. Sample preparation

Calcium–bismuth alloys were prepared using a laboratory arc-melter (MAM1, Edmund Bühler GmbH). Calcium dendritic pieces, purified by distillation, 99.99% metals basis (Aldrich, Stock No. 441872) and bismuth polycrystalline lumps, Puratronic®, 99.999% metals basis (Alfa Aesar, Stock No. 14442) were weighed in appropriate quantities and arc-melted together to achieve the nominal mole fractions of calcium x_{Ca} listed in Table 1.

Table 1
Calcium mole fractions x_{Ca} of arc-melted Ca–Bi alloys used for emf measurements, as weighed nominal values and as measured by DCP-AES chemical analysis.

Mole fraction, x_{Ca}	
Nominal	Measured
0.01	0.01
0.05	0.05
0.10	0.09
0.15	0.15
0.15	0.16
0.20	0.20
0.25	0.25
0.30	0.30
0.35	0.36
0.45	0.43
0.55	0.56
0.65	0.62
0.75	0.72
0.80	0.79
0.80	0.82
0.85	0.84
0.90	0.89
0.90	0.92
0.95	0.95
0.95	0.96
1.00	1.00

2.2. Emf measurements

Solid CaF_2 electrolyte for emf measurements was prepared by thoroughly mixing 500 g high-purity CaF_2 powder (Fisher Scientific, Stock No. C89-500), 5 g polyvinyl alcohol binder, and 250 mL de-ionized water. The mixture was dried in air for 24 h, ground into a fine powder with a mortar and pestle, and then uniaxially pressed at 30 MPa into a green pellet 75 mm × 17 mm in diameter and thickness. Seven holes 11.2 mm × 12 mm in diameter and depth were drilled into the green pellet; one in the center and six holes evenly spaced 25.4 mm from the center, Fig. 1. The green pellet was then fired under air atmosphere in a crucible furnace (Thermal Scientific) at 393 K for 8 h, 823 K for 12 h, and then 1273 K for 5 h to remove moisture, burn-out organic binder, and sinter, respectively. The final sintered CaF_2 pellets were ~98% theoretical density as estimated from measurements of their masses by electronic balance and of their volumes by digital calipers.

Arc-melted Ca–Bi alloys were machined into pellets 10 mm × 7 mm in diameter and thickness with 1.2 mm diameter holes through the center for the insertion of electrical leads.

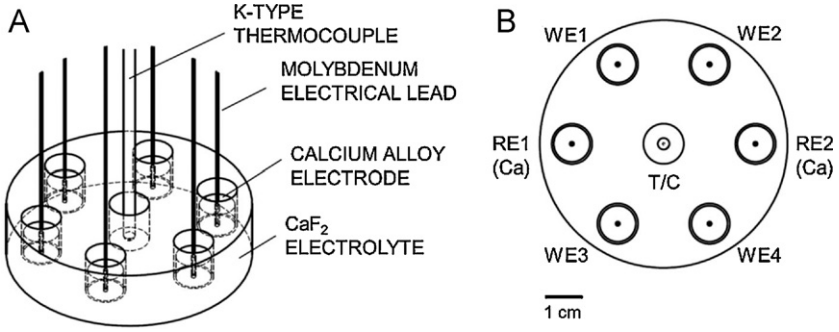

Fig. 1. Illustrations of the Ca(s)|CaF_2(s)|Ca(in Bi) cell used for emf measurements in (A) isometric view and (B) top view with the positions of the thermocouple (T/C), working electrodes (WEs), and reference electrodes (REs) indicated.

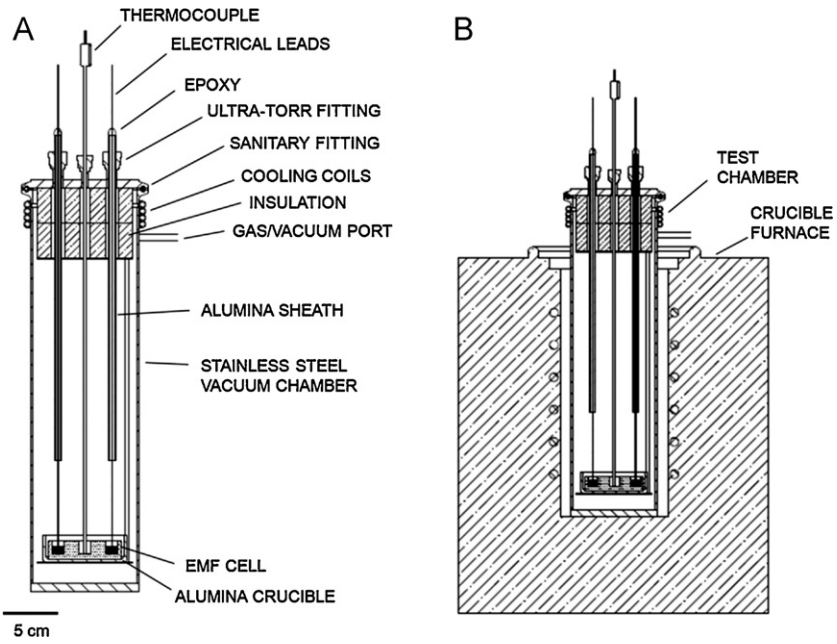

Fig. 2. Schematic cross-sectional diagrams of the emf measurement experimental set-up: (A) cell test chamber assembly and (B) test chamber loaded into a crucible furnace.

In each experiment, four Ca–Bi alloy working electrodes plus two pure Ca reference electrodes were placed into the sintered CaF_2 pellet and 1 mm diameter Mo wire leads inserted for electrical connection, as shown in Fig. 1.

The final assembly was completed under an inert argon atmosphere in a glove box (O_2 concentration < 1 ppm) to minimize the reaction of the cell components with oxygen gas and moisture. The assembled cell was then placed into an alumina crucible, the crucible inserted into a stainless steel vacuum chamber, the chamber sealed, and loaded into a crucible furnace, see Fig. 2. Next, the test chamber was evacuated to ~1 Pa and heated to and held at 393 K for 8 h to remove residual moisture in the system, purged with ~0.2 $cm^3\ s^{-1}$ (~10 mL min^{-1}) high-purity argon gas to prevent oxidation, and then heated to 1173 K to melt the samples and establish intimate contact between the electrode, electrolyte, and electrical leads. This procedure produced CaF_2 of requisite purity for making accurate electrochemical measurements, i.e., acceptable values of residual moisture content and of extent of conversion to the oxyfluoride, as evidenced by the fact that emf measurements made with high-purity single crystals were found to be in excellent agreement with those made with pellets.

The cell temperature was recorded using an ASTM type-K thermocouple and thermocouple data acquisition system (NI 9211, National Instruments). Emf data were collected upon cooling and reheating the cell between 723 K and 1173 K in 25 K steps, a period of ~1.5 h allowed for temperature equilibration at each step. The voltage between the reference and working electrodes for each couple was recorded using a potentiostat-galvanostat (Autolab PGSTAT302N, Metrohm AG) over a period of ~120 s after each temperature equilibration. The voltage between the two Ca reference electrodes was periodically monitored throughout each experiment and found to be within ±2 mV. All measurements were made at ambient pressure.

2.3. Chemical and structural characterization

The chemical compositions of the arc-melted Ca–Bi alloys were determined with a precision of ±2% of measured value using direct current plasma-atomic emission spectroscopy (DCP-AES) by an external vendor (Luvak Inc., Boylston, MA) according to the ASTM E 1097-07 standard. The results are given in Table 1.

Phase characterization of Ca–Bi alloys was performed by powder X-ray diffraction using a PANalytical X'Pert Pro Multipurpose Diffractometer with X'Celerator position sensitive detector and Cu-Kα radiation over 2θ angles 5–65°. Samples were prepared by grinding into a fine powder with a mortar and pestle in liquid nitrogen and mixed with a small amount of vacuum grease (Dow Corning 976V) to minimize oxidation.

2.4. Thermal analysis

Simultaneous differential scanning calorimetry (DSC) and thermal gravimetric analysis (TGA) were carried out using a STA 409 CD Skimmer (Netzsch Instruments). Arc-melted Ca–Bi samples (20–50 mg) were placed on tungsten foils within an alumina sample crucible to prevent reactions between calcium and alumina. Data were collected upon multiple dynamic heating/cooling cycles at a rate of 20 K min^{-1} under 0.3 cm^3 s (20 mL min^{-1}) high-purity flowing Ar gas.

3. Results and discussion

3.1. Emf measurements

Fig. 3 displays emf measurements made upon cooling and reheating of a cell containing Ca–Bi alloys, x_{Ca} = 0.20, 0.25, 0.30, and 0.35. In general, there is close agreement between emf values made during cooling and reheating. Fig. 4 shows the variation of emf with temperature and composition for selected Ca–Bi alloy compositions. In Fig. 4a, above the liquidus [liquid = liquid + $Ca_{11}Bi_{10}$(s)] emf varies linearly with temperature and increases monotonically as x_{Ca} decreases. Below the liquidus, calcium activity is invariant with composition and emf values fall onto a single line. In Fig. 4b, mole fractions x_{Ca} = 0.43 and 0.56 lie within the liquid + $Ca_{11}Bi_{10}$(s) two-phase region with identical emf values over the measured temperature range. At x_{Ca} = 0.62, which falls within

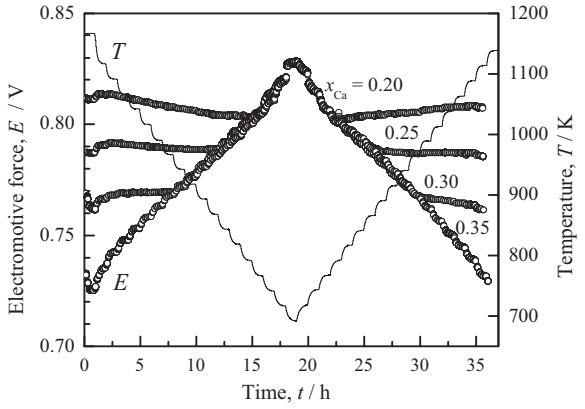

Fig. 3. Electromotive force and temperature measured as a function of time upon cooling and reheating a Ca (s)|CaF_2 (s)|Ca (in Bi) cell with Ca–Bi alloys x_{Ca} = 0.20, 0.25, 0.30, and 0.35.

the $Ca_{11}Bi_{10}$(s) + Ca_5Bi_3(s) two-phase region, the emf data are lower by ~100 mV. Finally, for calcium-rich solutions, $x_{Ca} > 0.62$, the measured emfs were nearly zero (within measurement error, ±2 mV).

From linear fits of the data presented in Fig. 4, the change in calcium partial molar entropy was calculated from the thermodynamic relation:

$$\Delta\bar{S}_{Ca} = -\left(\frac{\partial\Delta\bar{G}_{Ca}}{\partial T}\right)_P = zF\left(\frac{\partial E}{\partial T}\right)_P \quad (9)$$

and the change in calcium partial molar enthalpy from the Gibbs–Helmholtz relation,

$$\Delta\bar{H}_{Ca} = -T^2\left(\frac{\partial(\Delta\bar{G}_{Ca}/T)}{\partial T}\right)_P = zFT^2\left(\frac{\partial(E/T)}{\partial T}\right)_P \quad (10)$$

and the results are reported in Table 2. The change in partial molar entropy and enthalpy were assumed to be temperature-independent over the fitted range.

The thermodynamic data for Ca–Bi alloys at 873 K, 973 K, and 1073 K are summarized in Table 3. The activity of calcium in bismuth was calculated from the emf at each temperature and composition according to the following relationship,

$$\ln a_{Ca} = -\frac{zFE}{RT}. \quad (11)$$

From these data, the excess partial molar Gibbs energy of calcium was calculated by

$$\bar{G}^E_{Ca} = RT(\ln a_{Ca} - \ln x_{Ca}). \quad (12)$$

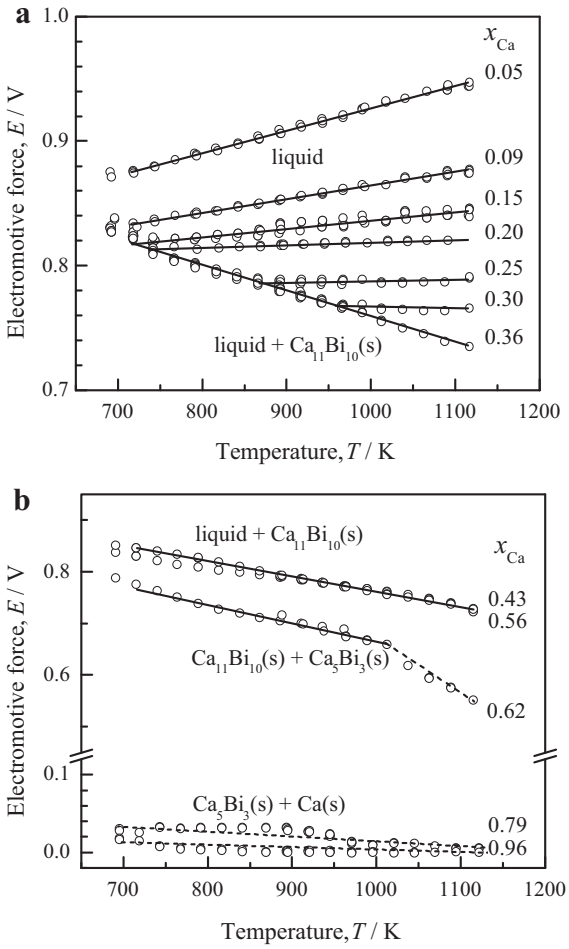

Fig. 4. Electromotive force as function of temperature upon cooling and reheating a Ca (s)|CaF_2 (s)|Ca (in Bi) cell with Ca–Bi alloys (a) x_{Ca} = 0.05–0.36 and (b) x_{Ca} = 0.43–0.96, where the solid lines are linear fits to the data and dashed lines a visual guide.

Fitting $\bar{G}^E_{Ca}$ data, the Gibbs–Duhem equation was used to estimate the excess partial molar Gibbs energy of bismuth by

$$\bar{G}^E_{Bi} = \int_0^{x_{Ca}} \frac{\bar{G}^E_{Ca}}{(1-x_{Ca})^2}\,dx_{Ca} - \frac{x_{Ca}\bar{G}^E_{Ca}}{1-x_{Ca}}. \quad (13)$$

Table 2
Change in partial molar entropy $\Delta\bar{S}_{Ca}$ and enthalpy $\Delta\bar{H}_{Ca}$ of calcium calculated from linear fits ($R^2 > 0.9$) to the electromotive force E versus temperature T data of Ca(s)|CaF_2(s)|Ca(in Bi) cells with Ca–Bi alloys x_{Ca} = 0.04–0.62, where the slopes and intercepts are $(\partial E/\partial T)_P$ and $T^2(\partial(E/T)/\partial T)_P$, respectively.

x_{Ca}	T (K)	$\partial E/\partial T$ (μV K^{-1})	$T^2(\partial(E/T)/\partial T)$ (mV)	$\Delta\bar{S}_{Ca}$ (J mol^{-1} K^{-1})	$\Delta\bar{H}_{Ca}$ (kJ mol^{-1})
0.04	716–1115	425	741	82.0	−143
0.05	716–1115	181	746	34.9	−144
0.09	716–1115	110	755	21.2	−146
0.16	717–1115	68	769	13.1	−148
0.20	737–1115	21	798	4.0	−154
0.25	868–1115	13	775	2.5	−150
0.30	958–1115	−13	780	−2.5	−151
0.36	716–1115	−205	964	−39.5	−186
0.43	716–1115	−231	994	−44.6	−192
0.56	716–1115	−296	1058	−57.2	−204
0.62	716–1063	−303	982	−58.4	−189

Table 3
Measured electromotive force E, natural log activity of calcium $\ln a_{Ca}$, measured excess partial molar Gibbs energy of calcium $\bar{G}^E_{Ca}$, Gibbs–Duhem estimated excess partial molar Gibbs energy of bismuth $\bar{G}^E_{Bi}$, and the estimated integral change in Gibbs energy ΔG of Ca–Bi alloys at 873 K, 973 K, and 1073 K as function of calcium mole fraction x_{Ca}.

x_{Ca}	E (V)			$\ln a_{Ca}$			$\bar{G}^E_{Ca}$ (kJ mol^{-1})			$\bar{G}^E_{Bi}$ (kJ mol^{-1})			ΔG (kJ mol^{-1})		
	873 K	973 K	1073 K	873 K	973 K	1073 K	873 K	973 K	1073 K	873 K	973 K	1073 K	873 K	973 K	1073 K
0.01	1.627	1.599	1.570	-43.3	−38.1	−34.0	−280	−271	−261	0	0	0	−2.4	−2.4	−2.3
0.05	0.903	0.921	0.939	−24.0	−22.0	−20.3	−152	−153	−154	−2	−2	−1	−9.0	−9.1	−9.0
0.09	0.850	0.861	0.872	−22.6	−20.5	−18.9	−147	−147	−147	−2	−2	−2	−15.0	−15.0	−14.9
0.15	0.829	0.835	0.841	−22.0	−19.9	−18.2	−146	−146	−145	−3	−3	−3	−24.0	−24.1	−24.0
0.16	0.830	0.836	0.842	−22.1	−19.9	−18.2	−147	−147	−146	−3	−3	−3	−25.7	−25.8	−25.7
0.20	0.816	0.818	0.820	−21.7	−19.5	−17.7	−146	−145	−144	−3	−3	−3	−31.5	−31.6	−31.5
0.25	0.788	0.788	0.788	−20.9	−18.8	−17.1	−142	−141	−140	−3	−4	−4	−38.0	−38.1	−38.2
0.30	0.785	0.769	0.766	−20.9	−18.3	−16.6	−143	−139	−137	−4	−5	−5	−45.3	−44.7	−44.7
0.36	0.785	0.765	0.744	−20.9	−18.2	−16.1	−144	−139	−134	−4	−5	−6	−54.3	−53.4	−52.5
0.43	0.792	0.769	0.745	−21.1	−18.3	−16.1	−147	−142	−136	−4	−6	−8	−65.6	−64.2	−63.1
0.56	0.799	0.769	0.740	−21.2	−18.4	−16.0	−150	−144	−138	−7	−7	−9	−86.8	−83.7	−81.1
0.62	0.723	0.674	0.672	−19.2	−16.1	−14.5	−136	−126	−125	−26	−34	−30	−94.0	−91.1	−89.2
0.72	0.006	0.005	0.002	−0.2	−0.1	−0.1	1	2	2	−280	−268	−264	−77.6	−73.7	−72.2
0.79	0.030	0.017	0.005	−0.8	−0.4	−0.1	−4	−1	1	−282	−267	−264	−62.5	−57.2	−54.5
0.82	0.036	0.035	0.018	−1.0	−0.8	−0.4	−6	−5	−2	−281	−266	−262	−55.0	−52.0	−48.6
0.84	0.027	0.015	0.014	−0.7	−0.4	−0.3	−4	−1	−1	−280	−265	−261	−48.0	−43.6	−42.7
0.89	0.001	0.001	0.002	0.0	0.0	0.0	1	1	1	−277	−262	−258	−29.9	−28.2	−27.8
0.92	0.002	0.001	0.000	−0.1	0.0	0.0	0	1	1	−274	−259	−254	−21.7	−20.1	−19.6
0.95	0.001	0.001	0.001	0.0	0.0	0.0	0	0	0	−270	−254	−249	−13.3	−12.5	−12.3
0.96	0.001	0.000	−0.001	0.0	0.0	0.0	0	0	1	–	–	–	–	–	–
1.00	0.000	0.000	0.000	0.0	0.0	0.0	0	0	0	–	–	–	–	–	–

Finally, the integral change in Gibbs energy was calculated by the following equation

$$\begin{aligned}\Delta G &= x_{Ca}\Delta\bar{G}_{Ca} + x_{Bi}\Delta\bar{G}_{Bi} \\ &= x_{Ca}(\bar{G}^E_{Ca} + RT\ln x_{Ca}) + x_{Bi}(\bar{G}^E_{Bi} + RT\ln x_{Bi})\end{aligned} \quad (14)$$

for the overall Ca–Bi alloy formation reaction,

$$x_{Ca}Ca(s) + (1 - x_{Ca})Bi(l) = Ca_xBi_{1-x}(l, s). \quad (15)$$

The data compiled in Table 3 are presented graphically in Fig. 5. In Fig. 5a, the measured emf is plotted as a function of calcium mole fraction in bismuth at temperatures 873 K, 973 K, and 1073 K. As the calcium mole fraction increases above $x_{Ca} > 0.01$, the emf drops precipitously from over 1.5 V to values less than 0.78 V at the liquidus ($x_{Ca} = 0.27$, 0.32, and 0.36 for $T = 873$ K, 973 K, and 1073 K, respectively). As expected, the emf is nearly constant through the two-phase region [liquid + $Ca_{11}Bi_{10}$(s)] up to $x_{Ca} = 0.52$ ($Ca_{11}Bi_{10}$), then decreases slightly in the $Ca_{11}Bi_{10}$(s) + Ca_5Bi_3(s) region, and finally drops to nearly zero at $x_{Ca} > 0.62$ (Ca_5Bi_3).

In Fig. 5b–e are plotted as function of calcium mole fraction at 873 K, 973 K, and 1073 K the values of calcium activity determined by emf measurements and the values of bismuth activity calculated by the Gibbs–Duhem equation, the excess partial molar Gibbs energy, and the integral change in Gibbs energy. Also shown for comparison are the coulometric titration results of Ca–Bi alloys at 1073 K obtained by Delcet et al. [5]. In general, the results of this work are in close agreement with those of Delcet, except for the bismuth activities (Fig. 5c), which are likely the result of inaccuracies associated with the Gibbs–Duhem estimation.

For comparison, the ideal Gibbs energy of mixing,

$$\Delta G^{id} = RT(x_{Ca}\ln x_{Ca} + x_{Bi}\ln x_{Bi}) \quad (16)$$

is also plotted at 873 K, 973 K, and 1073 K in Fig. 5e. As can be seen from comparison with Gibbs energy values calculated from emf measurements, Ca–Bi alloy formation exhibits mixing behavior indicative of strong negative deviation from ideality. This results in a higher cell voltage for a given degree of calciation and hence makes the system attractive for use in an energy storage device.

3.2. Structural characterization

A summary of crystal structures of known phases in the Ca–Bi system at ambient pressures is given in Table 4. Omitted from the table is the structure for Ca_2Bi, which was recently found to be an oxide of the form Ca_4Bi_2O [17].

Powder X-ray diffraction data collected on arc-melted Ca–Bi alloys are presented in Fig. 6. For $x_{Ca} < 0.35$, only the diffraction pattern of the bismuth trigonal phase, $Bi(R\bar{3}mH)$ is observed. Interestingly, evidence of this phase persists up to as high as $x_{Ca} = 0.75$, suggesting significant meta-stability of the $Bi(R\bar{3}mH)$ phase. Moreover, upon closer examination the (0 1 2) diffraction peak ($2\theta = 27.2^\circ$) broadens significantly upon increasing the calcium mole fraction, suggesting chemical disorder induced by Ca atomic substitution on the Bi site (crystallographic position) (Fig. 6b).

Evidence of the $Ca_{11}Bi_{10}$ phase begins to appear at $x_{Ca} = 0.45$ and is clearly present at $x_{Ca} = 0.55$. From $x_{Ca} = 0.65$ to 0.95, the Ca_5Bi_3 phase was identified, while the Ca(rt) phase can be identified only for $x_{Ca} \geq 0.85$. From these diffraction data, several peaks remained unidentified, specifically for $x_{Ca} = 0.65$ the peaks at $2\theta = 17.4^\circ$, 24.9°, 23.3°, 32.3°, and 50.0° and for $x_{Ca} = 0.85$ and 0.95 the peak at $2\theta = 26.1^\circ$.

Notably absent from the diffraction data collected is any evidence of $CaBi_2$ and $Ca_{16}Bi_{11}$ for which there are published crystal structures. The reported preparation of $CaBi_2$ for crystal structure determination includes the annealing of the alloy in a sealed iron crucible for one month at 723 K [12]. Similarly, $Ca_{16}Bi_{11}$ was prepared by annealing at 1173 K for one month in a sealed tantalum crucible [14]. It may be that the formation of these alloys is kinetically inhibited and therefore not readily observable in samples prepared by arc-melting.

3.3. Thermal analysis

Representative DSC scans collected upon heating and cooling of Ca–Bi alloys are given in Fig. 7, in which major transitions are designated by roman numerals (I–VII). A summary of transition temperatures T_{trs} and enthalpies $\Delta_{trs}H$ averaged over multiple heating and cooling cycles is given in Table 5.

The average measured fusion temperature T_{fus} and enthalpy $\Delta_{fus}H$ of pure Bi was 524(23) K and 10.2(7) kJ mol^{-1}, which are

Table 4
Summary of reported crystal structures in the Ca–Bi system.

Phase	x_{Ca}	T (K)	ρ (g cm^{-3})	Space group (Pearson symbol)	Lattice parameters (nm)	(°)	Refs.
(Bi)	0.00	298	9.81	$R\bar{3}mH$ (hR2)	a = 0.455 b = 0.455 c = 1.186	α = 90 β = 90 γ = 120	[11]
$CaBi_2$	0.33	298	8.24	$Cmcm$ (oS12)	a = 0.470 b = 1.705 c = 0.461	α = 90 β = 90 γ = 90	[12]
$Ca_{11}Bi_{10}$	0.52	298	6.33	$I4/mmm$ (tI84)	a = 1.222 b = 1.222 c = 1.779	α = 90 β = 90 γ = 90	[13]
$Ca_{16}Bi_{11}$	0.59	298	5.49	$P\bar{4}2_1m$ (tP8)	a = 1.249 b = 1.249 c = 1.143	α = 90 β = 90 γ = 90	[14]
Ca_5Bi_3	0.63	298	5.30	$Pnma$ (oP32)	a = 1.272 b = 0.967 c = 0.843	α = 90 β = 90 γ = 90	[15]
(Ca)rt	1.00	298	1.52	$Fm\bar{3}m$ (cF4)	a = 0.559 b = 0.559 c = 0.559	α = 90 β = 90 γ = 90	[16]
(Ca)ht	1.00	740	1.48	$Im\bar{3}m$ (cI2)	a = 0.448 b = 0.448 c = 0.448	α = 90 β = 90 γ = 90	[16]

slightly less than the reported values of 545 K and 11.2 kJ mol^{-1} [18]. Measurement imprecision was likely due to use of high heating/cooling rates (20 K min^{-1}). To minimize equipment damage due to the high reactivity of pure calcium, only a single measurement was made, which yielded values of T_{fus} = 1110 K and $\Delta_{fus}H$ = 3.8 kJ mol^{-1}, both substantially lower than the reported values of 1115 K and 8.5 kJ mol^{-1} [18]. Further thermal analysis using sealed crucibles is needed to obtain accurate liquidus values, as the high reactivity and volatility of calcium at high temperatures and high calcium activities impeded the acquisition of accurate and reproducible data in the present study.

3.4. Phase diagram

The most recent Ca–Bi phase diagrams were reported by Notin et al. [19] who used NANCYUN software to optimize direct reaction calorimetry [20] and emf data [5] and by Okamoto [21] who used primarily the thermal analysis data reported by Smirnov and Rudnichenko [22]. From these phase diagrams, reactions were assigned to the observed transition behavior reported in the previous section and compared with prior studies, Table 6.

These previous phase diagrams report a $CaBi_3$ phase that melts at ~790 K resulting in the peritectic transition

$$L + Ca_{11}Bi_{10} \underset{790\,K}{\overset{T_{trs}}{\longleftrightarrow}} CaBi_3; \quad (III^*)$$

however, no structural evidence of $CaBi_3$ exists. This work suggests that the transition observed at ~790 K is not $CaBi_3$ melting, but an allotropic (solid–solid) phase transition of $Ca_{11}Bi_{10}$,

$$Ca_{11}Bi_{10}(ht) \underset{767\,K}{\overset{T_{trs}}{\longleftrightarrow}} Ca_{11}Bi_{10}(rt) \quad (III)$$

which is evident from the results given in Table 5 (transition III), in which the $\Delta_{trs}H$ approaches a maximum at $0.43 < x_{Ca} < 0.56$, i.e.

Table 5
Summary of transition temperatures T_{trs} (K) and enthalpies $\Delta_{trs}H$ (kJ mol^{-1}) measured by differential scanning calorimetry and averaged over multiple heating and cooling cycles.

Transition	x_{Ca}	0.00	0.09	0.20	0.30	0.36	0.43	0.56	0.62	0.72	0.82	0.92	1.00
I	T_{trs}	524(23)	–	–	–	–	–	–	–	–	–	–	–
	$\Delta_{trs}H$	10.2(7)	–	–	–	–	–	–	–	–	–	–	–
II	T_{trs}	–	537(5)	535(7)	533(5)	537(9)	530(3)	526(4)	–	–	–	–	–
	$\Delta_{trs}H$	–	7.5(9)	6.1(8)	3.2(7)	2.6(4)	0.5(2)	–	–	–	–	–	–
III	T_{trs}	–	–	–	767(1)	770(11)	768(7)	763(2)	–	–	–	–	–
	$\Delta_{trs}H$	–	–	–	0.9(2)	1.3(4)	1.5(2)	0.3(2)	–	–	–	–	–
IV	T_{trs}	–	–	–	–	–	–	1367(19)	–	–	–	–	–
	$\Delta_{trs}H$	–	–	–	–	–	–	1.2(3)	–	–	–	–	–
VI	T_{trs}	–	–	–	–	–	–	–	–	–	702(2)	723(15)	715(2)
	$\Delta_{trs}H$	–	–	–	–	–	–	–	–	–	0.3(1)	5.8(22)	17.7(1)
VII	T_{trs}	–	–	–	–	–	–	–	–	1071(7)	1065(5)	1084(8)	–
	$\Delta_{trs}H$	–	–	–	–	–	–	–	–	0.4(2)	2.7(6)	3.6(10)	–
VIII	T_{trs}	–	–	–	–	–	–	–	–	–	–	–	1110
	$\Delta_{trs}H$	–	–	–	–	–	–	–	–	–	–	–	3.8
Liquidus	T_{trs}	–	646	702	–	–	–	1474	–	–	–	–	–

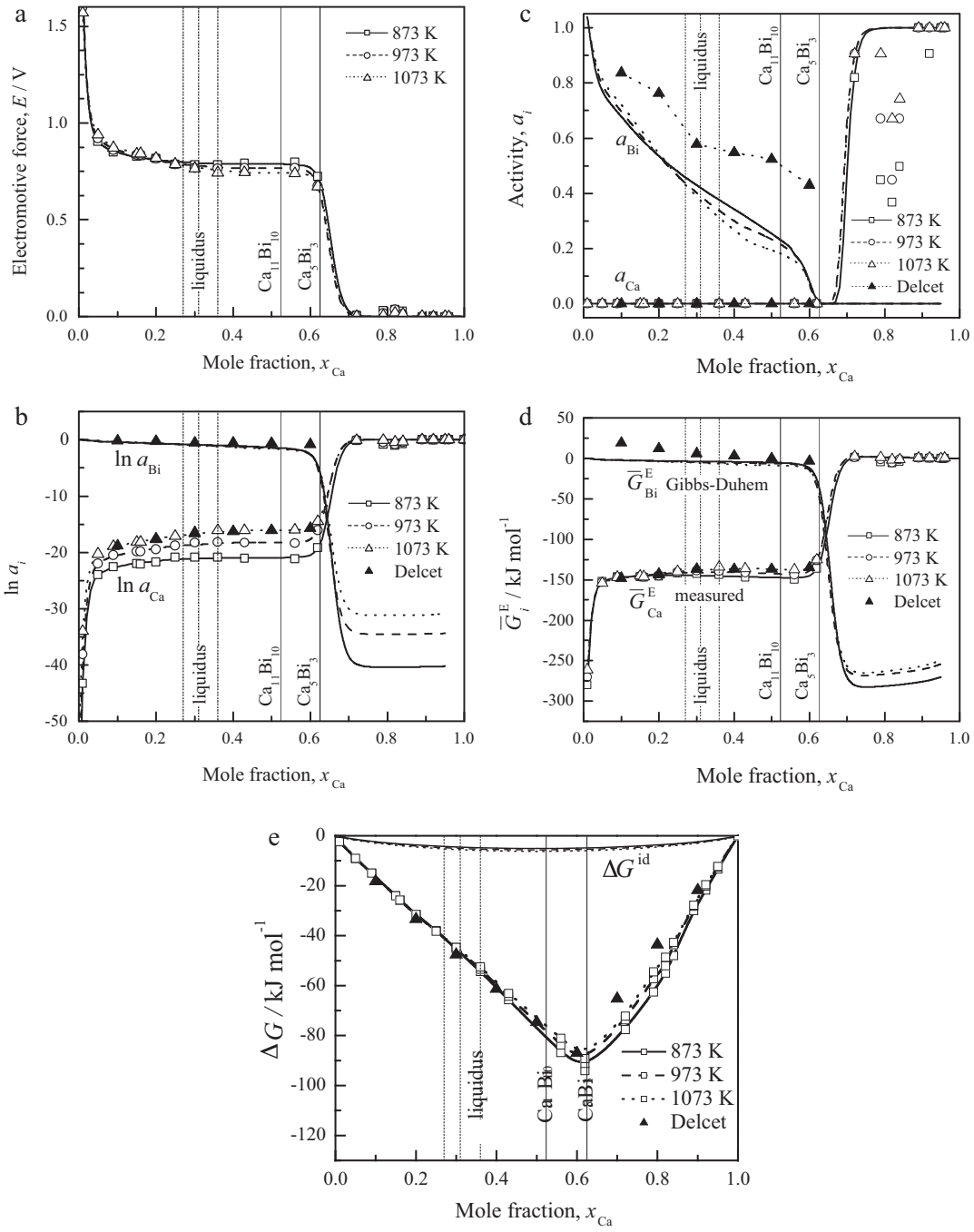

Fig. 5. Plots of the (a) measured electromotive force E measured in a Ca(s)|CaF_2(s)|Ca(in Bi) cell; (b) natural logarithm activity and (c) activity of calcium a_{Ca} and bismuth a_{Bi}; (d) excess partial molar Gibbs energy of calcium $\bar{G}^E_{Ca}$ (measured) and of bismuth $\bar{G}^E_{Bi}$ (Gibbs–Duhem); and (e) integral change in Gibbs energy ΔG and ideal Gibbs energy of mixing ΔG^{id} as a function of calcium mole fraction in bismuth x_{Ca} at temperatures 873 K, 973 K, and 1073 K. The coulometric titration results on Ca–Bi alloys at 1073 K obtained by Delcet et al. [5] are shown for comparison.

in the vicinity of $Ca_{11}Bi_{10}$ (x_{Ca} = 0.52). This assertion also leads to a modification of the eutectic transition reported at ~540 K,

$$L \underset{540\,K}{\overset{T_{trs}}{\longleftrightarrow}} (Bi) + CaBi_3 \qquad (II^*)$$

to the new eutectic transition forming the room temperature phase of $Ca_{11}Bi_{10}$,

$$L \underset{534\,K}{\overset{T_{trs}}{\longleftrightarrow}} (Bi) + Ca_{11}Bi_{10}(rt). \qquad (II)$$

A revised Ca–Bi binary phase diagram is proposed in Fig. 8. Liquidus data were obtained from emf results for x_{Ca} = 0.05–0.36 (Table 2), where the liquidus temperatures were estimated from the intersection of the (liquid) and (liquid + solid) lines fit to emf data as a linear function temperature for each composition x_{Ca}.

The crystal structure of the $CaBi_2$ phase is reported [12] and therefore also indicated in the phase diagram. Though not observed by powder X-ray diffraction analysis, preliminary scanning electron microscopy (SEM) and energy dispersive spectroscopy (EDS)

Table 6
Reactions assigned to the transition data presented in Table 5 and comparison to previous reports by Okamoto [21] and Notin et al. [19]. Asterisks (*) indicate transitions proposed for reclassification.

Transition	Reaction	T_{trs} (K) Okamoto	Notin	This study	Type
I	L = (Bi)	544	544	524(23)	Fusion
II*	L = (Bi) + $CaBi_3$	543	541	–	Eutectic
II	L = (Bi) + $Ca_{11}Bi_{10}$(rt)	–	–	534(5)	Eutectic
III*	L + $Ca_{11}Bi_{10}$ = $CaBi_3$	778	799	–	Peritectic
III	$Ca_{11}Bi_{10}$(ht) = $Ca_{11}Bi_{10}$(rt)	–	–	767(3)	Allotropic
IV	L + Ca_5Bi_3 = $Ca_{11}Bi_{10}$(ht)	1348	1357	1367(19)	Peritectic
V	L = Ca_5Bi_3	1623	1629	–	Congruent
VI	L = Ca_5Bi_3 + (Ca)ht	1093	1057	1073(8)	Eutectic
VII	(Ca)ht = (Ca)rt	716	–	713(15)	Allotropic
VIII	L = (Ca)ht	1115	1115	1110	Fusion

chemical analysis of arc-melted samples suggested the presence of $CaBi_2$. A complete equilibrium phase diagram of the Ca–Bi system including the $CaBi_2$ phase will require a reclassification of transitions II and III from those proposed here to the following:

$$L \underset{534K}{\overset{T_{trs}}{\longleftrightarrow}} (Bi) + CaBi_2 \qquad (II^{\dagger})$$

$$L + Ca_{11}Bi_{10}(ht) \underset{767\,K}{\overset{T_{trs}}{\longleftrightarrow}} CaBi_2. \qquad (III^{\dagger})$$

Also not observed in this work, but indicated in the phase diagram, is $Ca_{16}Bi_{11}$ for which a crystal structure is reported [14]. The Ca_2Bi phase reported by Okamoto, shown to be Ca_4Bi_2O

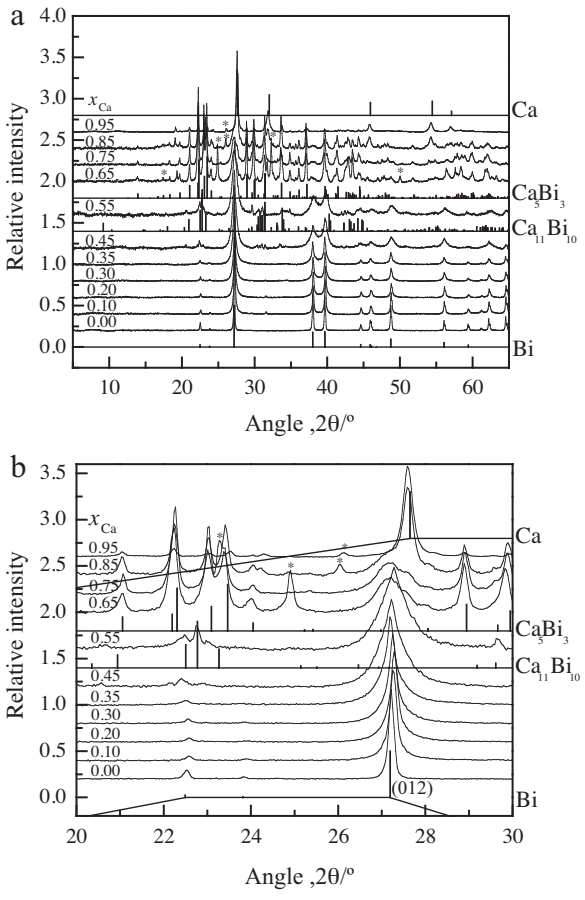

Fig. 6. Powder X-ray diffraction patterns collected on arc-melted Ca–Bi alloys x_{Ca} = 0.00–0.95: (a) full pattern, 2θ = 5–65° and (b) zoomed view, 2θ = 20–30°. Data are presented with baseline subtractions and 0.4 offsets in relative intensity. The asterisks (*) represent unidentified peaks.

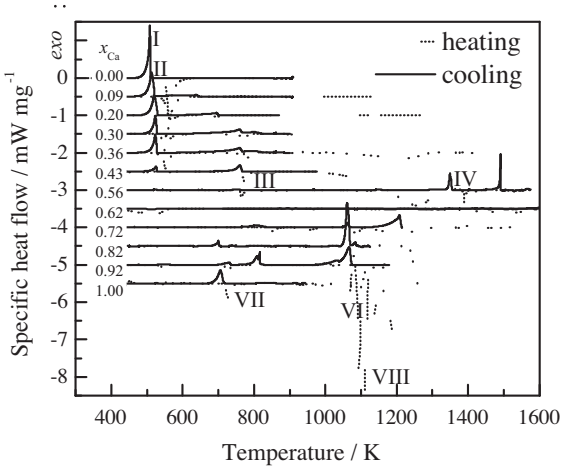

Fig. 7. Representative differential scanning calorimetry data collected upon heating and cooling at 20 K min^{-1} for Ca–Bi alloy compositions x_{Ca} = 0.00–1.00, major transitions are designated by Roman numerals (I–VII). Data are presented with baseline subtraction and 0.5 mW mg^{-1} offsets.

[17] was omitted here. Above x_{Ca} > 0.63, liquidus temperatures remain uncertain due to difficulties with measuring Ca–Bi alloys with high mole fractions of calcium at high temperatures. Lastly, the eutectic transition at 541 K was extended by a dotted line past x_{Ca} = 0.52 due to the evidence of a metastable (Bi) phase

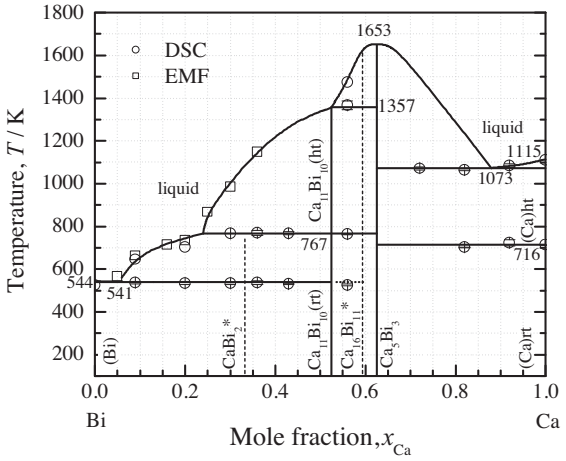

Fig. 8. Proposed revised Ca–Bi binary phase diagram based upon differential scanning calorimetry (DSC) and electromotive force (emf) measurements. The asterisks (*) represent phases not observed in this work.

in this region by both powder X-ray diffraction and thermal analysis.

4. Conclusions

From this study it was determined that an electrochemical energy storage device with positive calcium and negative bismuth electrodes, operated at temperatures of 873–1073 K would have a nominal theoretical discharge voltage of ~0.77 V and be capable of discharging calcium into bismuth up to a maximum degree of alloying of $x_{Ca} = 0.62$. While the Ca–Bi system yields a practical voltage for electrochemical energy storage, the high reactivity of calcium and its solubility in molten salt electrolytes represent significant engineering challenges.

Acknowledgments

The authors would like to thank Professors George Kipouros and Geir Martin Haarberg for their helpful advice on making emf measurements in cells fitted with solid electrolytes. The financial support of the US Department of Energy, Advanced Research Projects Agency-Energy (Award No. DE-AR0000047) and TOTAL, S.A. is gratefully acknowledged.

References

[1] A.S. Dworkin, H.R. Bronstein, M.A. Bredig, J. Phys. Chem. 66 (3) (1962) 572.
[2] G.M. Haarberg, J. Thonstad, J. Appl. Electrochem. 19 (6) (1989) 789.
[3] J.N. Pratt, Metall. Mater. Trans. A 21 (5) (1990) 1223.
[4] C. Wagner, J. Electrochem. Soc. 115 (9) (1968) 933.
[5] J. Delcet, A. Delgado-Brune, J.J. Egan, in: Y.A. Chang, J.F. Smith (Eds.), Calculation of Phase Diagrams and Thermochemistry of Alloy Phases, Proc. AIME, Fall Meet, 17–18 September, 1979, AIME, 1979, p. 275.
[6] J. Delcet, J.J. Egan, J. Less-Common Met. 59 (2) (1978) 229.
[7] J. Delcet, J.J. Egan, Metall. Trans. B 9 (4) (1978) 728.
[8] J. Delcet, R.J. Heus, J.J. Egan, J. Electrochem. Soc. 125 (3) (1978) C161.
[9] J. Delcet, R.J. Heus, J.J. Egan, J. Electrochem. Soc. 125 (5) (1978) 755.
[10] R.W. Ure, J. Chem. Phys. 26 (1957) 1363.
[11] P. Cucka, C.S. Barrett, Acta Crystallogr. 15 (1962) 865.
[12] F. Merlo, M.L. Fornasini, Mater. Res. Bull. 29 (2) (1994) 149.
[13] K. Deller, B. Eisenmann, Z. Naturforsch. 31b (1976) 29.
[14] E.A. Leon-Escamilla, W.-M. Hurng, E.S. Peterson, J.D. Corbett, Inorg. Chem. 36 (1997) 703.
[15] M. Martinez-Ripoll, A. Haase, G. Brauer, Acta Crystallogr. B 30 (1974) 2004.
[16] B.T. Bernstein, J.F. Smith, Acta Crystallogr. 12 (1959) 419.
[17] S. Xia, S. Bobev, J. Alloys Compd. 427 (2007) 67.
[18] D.R. Lide (Ed.), CRC Handbook of Chemistry and Physics, 84th ed., CRC Press, Boca Raton, Florida, 2003 (Section 6).
[19] M. Notin, J. Mejbar, A. Bouhajib, J. Charles, J. Hertz, J. Alloys Compd. 220 (1995) 62.
[20] A. Bouhajib, Doctorat, Université de Nancy I, Sep., 1990.
[21] H. Okamoto, in: T.B. Massalski (Ed.), Binary Phase Diagrams, 2nd ed., ASM International, 1990, p. 720.
[22] M.P. Smirnov, V.E. Rudnichenko, Zh. Neorg. Khim. 8 (6) (1963) 1402.